Fastener-Free Low-Slope Roofing Systems: Can They Resist Wind Uplift?

By Dr. A. Baskaran, PEng; Jay Current, Bona Murty, Hiroshi Tanaka, and Jun Wu

Editor's Note: This article is republished from the Proceedings of the RCI 2010 International Convention and Trade Show.

ABSTRACT

A type of built-up roofs known as adhesive-applied roofing systems (AARS) uses no fasteners for component attachment. All of the AARS components (e.g., insulation board, cover board, and membranes) are integrated through the application of adhesives. Since there are no metal fasteners through which moisture migration and thermal bridging might normally travel, AARS eliminates these. Moisture in the roof envelope can generally lead to material deterioration, structural integrity problems, and the growth of mold. Even though AARS are being used, there is no dynamic test standard available to quantify their wind uplift performance.

Recently, the National Research Council of Canada (NRC) completed a five-year project, "Development of Wind Uplift Standard for Adhesive-Applied Low-Slope Roofing Systems," in collaboration with industries, universities, and the government. The project has three major experimental tasks:

1. Uplift testing – simulating the vertically induced tensile loading;
2. Peel testing – simulating shear loading; and
3. Full-scale testing – simulating the wind uplift loading.

The experimental investigation tested over 500 specimens for tensile loading and shear loading. Additionally, more than 40 full-scale mock-ups were constructed using steel deck and polyisocyanurate insulation with various adhesives (type, quantity, and application method), cover boards, and membranes. Mock-ups were subjected to both static and dynamic wind-loading conditions. Experimental data showed similarity in failure modes and variations in wind uplift ratings. Data show that among the mock-ups, the weakest link varied, depend-

FIELD APPLICATION

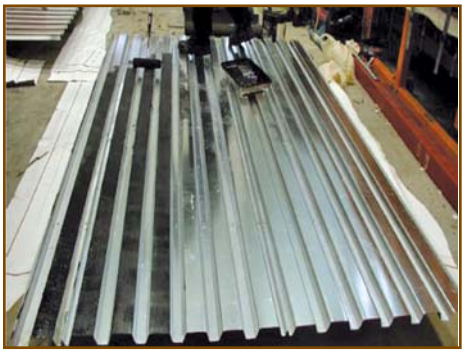

STEEL DECK INSTALLATION

VAPOR BARRIER INSTALLATION

ISO INSTALLATION

COVER BOARD INSTALLATION

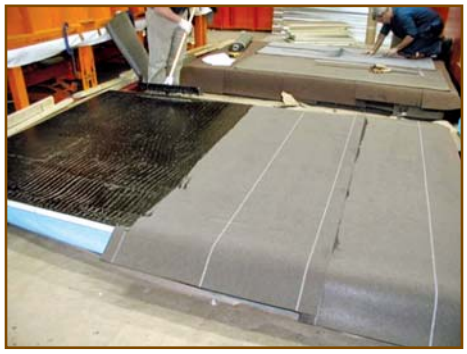

BASE SHEET INSTALLATION

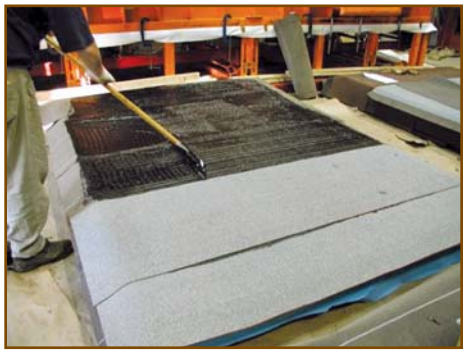

CAP SHEET INSTALLATION

Figure 1 – Field application and mock-up preparation.

ing on the type of adhesives used and the component arrangements. This paper presents and discusses the data from this experimental investigation and the development of a new wind uplift standard for AARS.

(To respect space limitations, this paper presents the data in an executive summary form. Details of the experimental program and draft version of the ASTM work items and CSA A123.21-04 standard updates are available upon request from the authors.)

INTRODUCTION

In a conventional roof assembly, the roof membrane is placed above the insulation and exposed to environmental forces, such as wind and rain. When all of the roof's components are fixed using fasteners to form a system, it can be classified as a mechanically attached roofing system (MARS). As an alternative to MARS, AARS are another type of built-up roofs that use adhesives to integrate all components such as insulation board, cover board, and membranes to form a compact roof system. If a compact roofing system uses a combination of fastener and adhesive to integrate its components, then it can be classified as a fully bonded system.

Figure 1 illustrates a typical mock-up construction and field photograph of AARS with modified bituminous membrane as the roof cover. Claims have been made that AARS offer several advantages over MARS. Since metal fasteners are not used in the system, thermal bridging and moisture migration can be minimized. The existence of the moisture travel path, such as fastener holes, is critical for moisture transport into the building envelope (Hens *et al.*, 1995). In a building envelope, moisture can lead to material deterioration, structural integrity problems, and excessive mold growth. AARS can also eliminate corrosion problems that occur on metal fasteners in the MARS, which may cause premature roof failure. Besides these advantages, AARS also offer less air intrusion compared with MARS. AARS installations are labor-intensive. Quality assurance and quality control during adhesive application, component slippage (e.g., some adhesives can soften at elevated temperature), and relatively longer curing time (most manufacturers recommend a minimum of 21 days) are some of the concerns related to AARS.

Figure 2 shows a force dissipation diagram between AARS and MARS. AARS and MARS respond differently to wind uplift

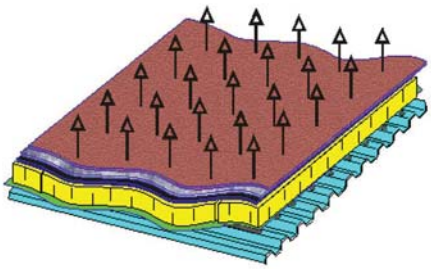

RIGID ROOF SYSTEM RESPONSE

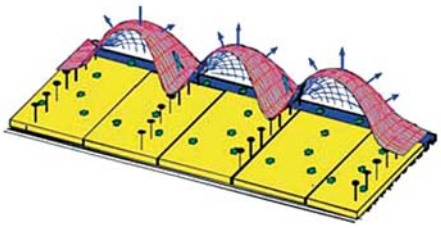

FLEXIBLE ROOF SYSTEM RESPONSE

RIGID ROOF SYSTEM FAILURE

FLEXIBLE ROOF SYSTEM FAILURE

Figure 2 – Wind uplift responses of MARS and AARS.

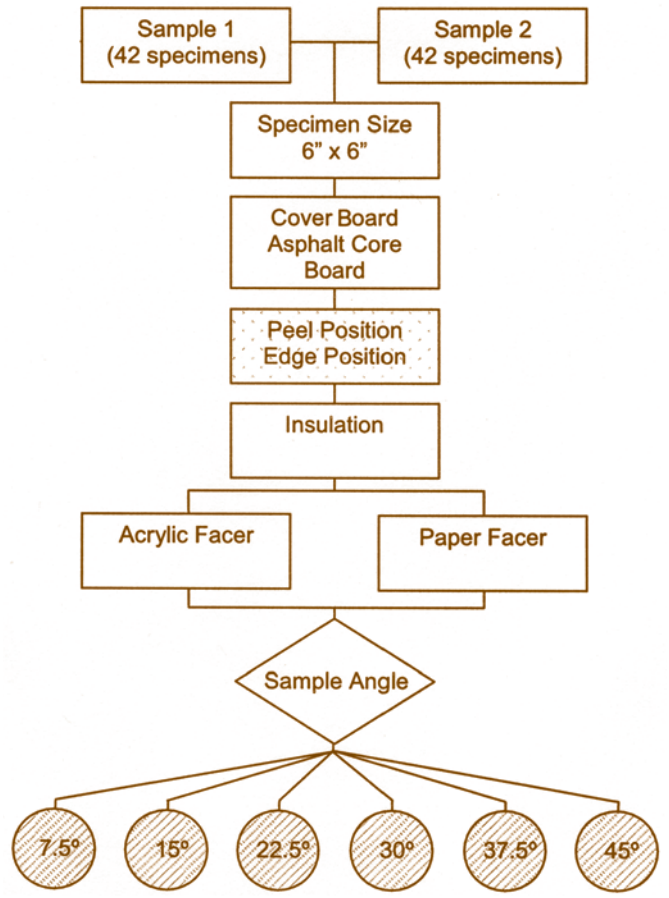

Figure 3 – Test matrix for peel testing by simulating shear loading.

forces. The AARS wind uplift performance can be classified as phonemic load transfer, in which all components unite and share the wind uplift forces. For MARS, the performance can be classified as structural load transfer or linear load path in which most of the membrane's tension is transferred to the structural deck through fasteners. In the AARS, wind loads are distributed over a roof area. As a result of this response variation, one should apply different methodology to determine the wind uplift resistance. Although AARS have been in use commercially in the North American roofing market, there is no existing dynamic test standard to quantify their wind uplift resistance. Therefore, a collaborative research project and comprehensive study of the AARS wind uplift resistance performance was recently completed by the NRC. This is a joint project with the Natural Sciences and Engineering Research Council (NSERC) that involves NRC, the University of Ottawa, roofing manufacturers, and contractors. This article presents the development of test protocols and experimental observations.

SMALL-SCALE PEEL TESTING BY SIMULATING SHEAR LOADING (WU, 2008)

Determination of Appropriate Peel Angle for Standardized Test Protocol

Outlined in *Figure 3* is the breakdown of the experimental conditions used to determine an appropriate peel angle in evaluating the resistance of AARS specimens against shear loading. The peel angle is the angle at which the force is being applied. Note that the specimens are replications of the same configuration, and they are sized at 6 in x 6 in (152 mm x 152 mm). All specimens were made of an asphalt core board and either acrylic facer (AF) or paper facer (PF) for insulation.

To investigate the effects of different peel angles on peel resistance, six different peel angles were examined: 7.5°, 15°, 22.5°, 30°, 37.5°, and 45°. The peel resistance data of the specimens at six different peel angles are presented in *Figure 4*. The x-axis shows the peel angle (θ), while the y-axis is showing the corresponding peel resistance. Each curve is made up of three distinct segments: Segment 1 = 7.5° to 15°, Segment 2 = 15° to 30°, and Segment 3 = 30° to 45°. Peel resistance is decreasing as the peel angle is increasing. This is mainly because the vertical tensile force acting on the specimen is increasing with the peel angle. The most rapid slope change is within segment 2 of each curve. This indicates a rapid change in peeling force related to the angles in this range and is called the effective angle range. Peeling resistance is most sensitive to changes in peel angle over the effective angle range. Angles less than 15° or more than 30° would have smaller effects on the peel resistance. The range of angles between 15° and 30° is important to zone in on for the development of standardized peel test methods to apply to future wind design guides for AARS. It is important, therefore, to develop a generalized curve that could be used to predict peel resistance performance under different peel angles.

A generalized peel-angle curve for peel resistance of AARS specimens is also illustrated in *Figure 4*. The data points for the generalized curve were obtained by averaging the curve data points of the specimens that use a paper facer insulation and asphaltic core board combination (PF/ACB), and the one with the acrylic facer insulation and asphaltic core board combination (AF/ACB). For example, at angle 7.5°, the peel resistance ratio is 1.95 for the AF/ACB curve and 1.1 for the PF/ACB curve. The peel resistance ratio for the generalized curve is [1.95 + 1.1]/2 = 1.51. All curves intersect at the reference angle of 15°. There is a significant difference in curves for angles less than the reference angle; however, peel resistance does not differ much at angles greater than the reference angle. The generalized curve could be applied to calculate the peel resistance at various angles after obtaining the peel resistance at 15°. Based on this analysis, the present study

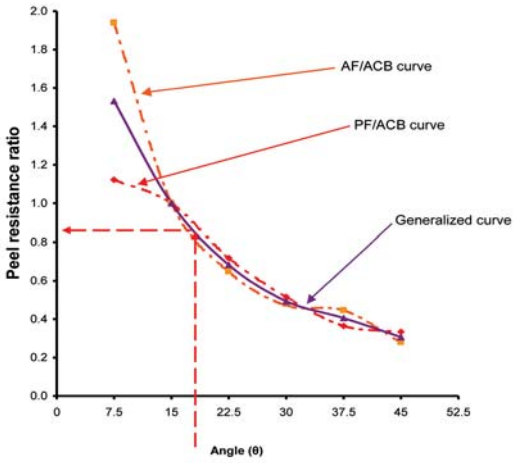

Figure 4 – Development of generalized curve for peel testing.

Figure 5 – Weakest link under shear loading; a summary of failure mode investigation.

proposes 15° as the appropriate angle for the standard test method.

Weakest Link Under Peel Loading – Summary of Failure Mode Investigation

Figure 5 indicates that over a half (53%) of the failures occurred in cover board (CB) components and 37% in the insulation component, leaving about 10% due to adhesives. These results suggest that the CB component is the weakest link, followed by the insulation, in AARS performance under wind uplift. Overall, CB seems to have a higher probability of failing under the current peel-test conditions. The high frequency of fiber board (FB) failure was the biggest contributing factor as to why CB was the weakest link in the samples examined. It is reasonable to consider that if ACB materials were used for the CB component with different insulation for AARS, most failures would have occurred in the insulation layer. This means that when the wind uplift acts on AARS, the weakest link is in the insulation layer if ACB is used as the cover board. However, if FB is used for the cover board, the failure is likely to occur in the cover board layer. In summary, delamination represents the weakest link for insulation components, and brittle failure represents the highest frequency for CB components under wind-peel force.

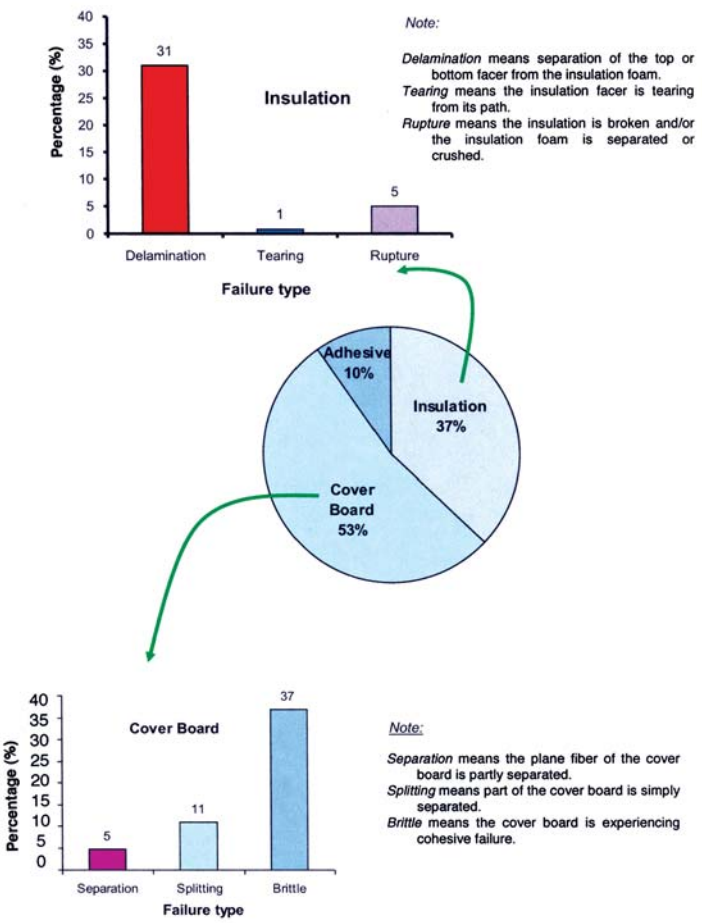

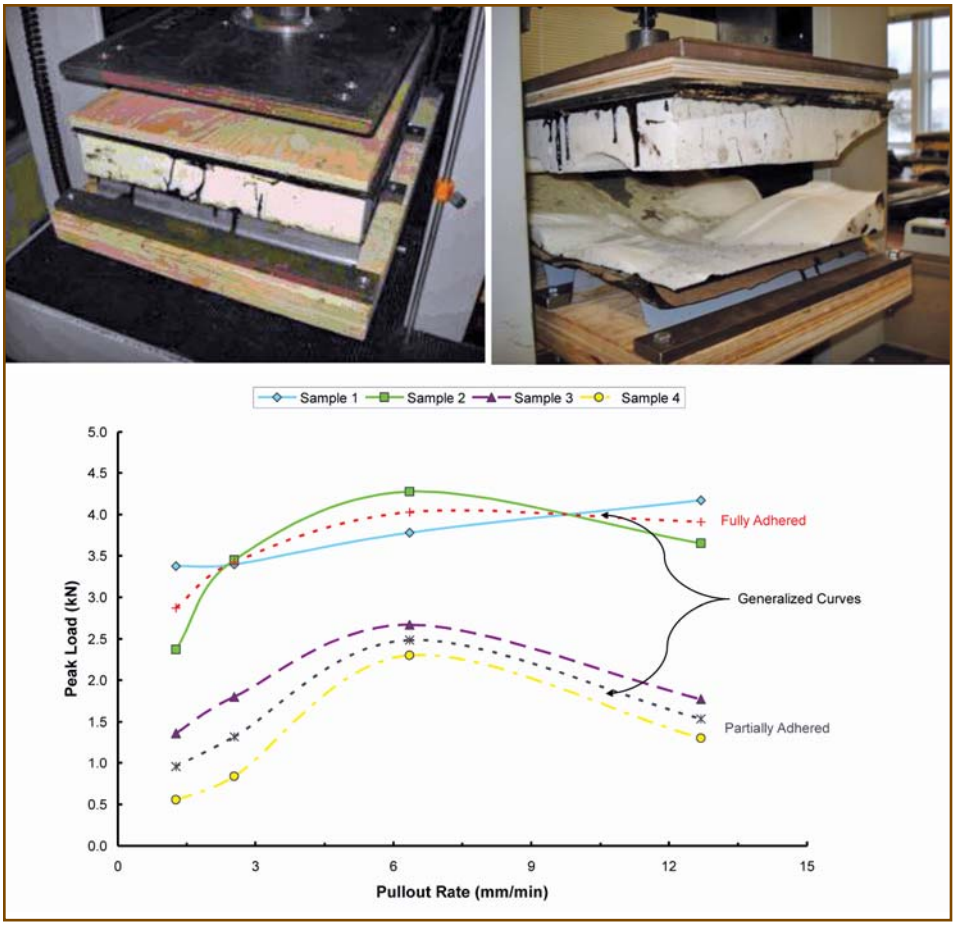

Figure 6 – Development of generalized curve for uplift resistance of AARS.

SMALL-SCALE UPLIFT TESTING BY SIMULATING TENSILE LOADING (CURRENT, 2009)

Determination of Appropriate Uplift Rate for Standardized Test Protocol

Figure 6 shows the measured peak loads at four different uplift rates. The x-axis shows the uplift rate in mm/min where a maximum load that the sample reached is shown in the y-axis. Note that each sample datum represents an average of eight specimens. The data were grouped corresponding to two sets: namely, fully adhered (FA) and partially adhered (PA). Samples in which components were fully adhered had high resistance to the applied tensile loading compared to the partially adhered samples, regardless of the uplift rate, indicating that an increase in the adhered area increases the uplift resistance.

There is a minimal difference between the peak loads of the two samples in each set, which led to an approach in which the corresponding peak loads were averaged to obtain generalized data for each uplift rate. Two generalized curves were obtained: one for a PA set and the other for a FA set. From the generalized curves, it is clear that there is an increase in peak load from 0.05 in/min (1.27 mm/min) to 0.25 in/min (6.35 mm/min), followed by a decline as the speed is increased even further. Based on these findings, it appears that the optimum rate for characterizing uplift resistance is 0.25 in/min (6.35 mm/min).

Weakest Link Under Tensile Loading – Summary of Failure Mode Investigation

Elastic energy (the energy within the elastic range) was calculated to determine the uplift resistance of each specimen with its respective insulation and cover board combination. An average of the elastic energy displayed by each material combination is represented in *Figure 7*. The elastic energy values presented are an average from the specimens of the particular configuration type. The data were grouped corresponding to two sets: namely, fully adhered (FA) and partially adhered (PA). Consistent failure of specimens was observed in a very specific range of about 2.0 – 2.4 J of elastic work, regardless of sample, material, or type of adhesion.

There were two exceptions to this observation. First, the PF/ACB (FA) specimens were able to absorb double the amount of energy (~ 4 J) before their failure. Second, all specimens of FB (PA) cover board combinations fail around only 1 J of elastic energy, with PF/FB (PA) being the worst. These observations confirm the conclusion that the best material combination is PF/ACB (FA), and the worst material combination is PF/FB (PA). It should also be noted that the drastic drop in uplift resistance toward energy input from PF/ACB (FA) to PF/FB (PA) illustrates that it is the difference in the cover board that leads to premature failure, considering the insulation remains constant. During failure-plane analysis, there were three failure planes found: adhesive failure, facer rupture, and facer delamination.

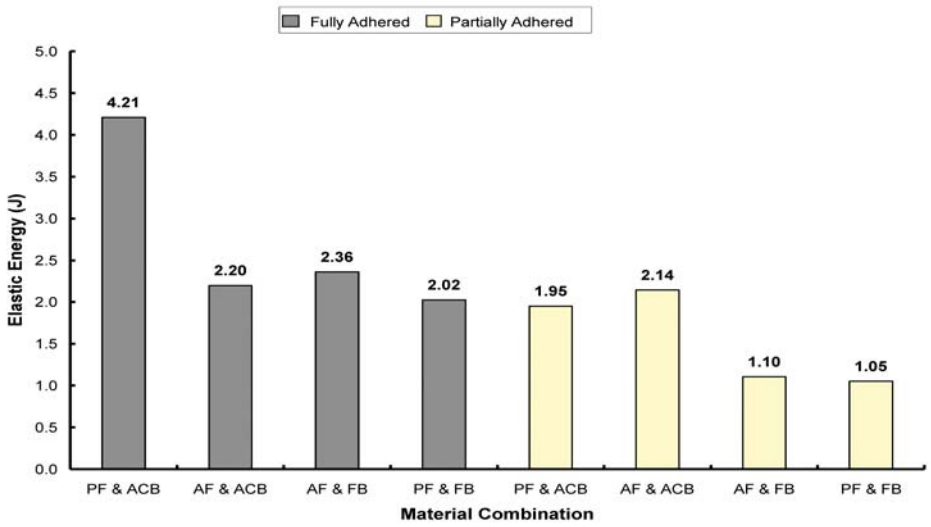

Figure 7 – Weakest link under tensile loading; a summary of component investigation.

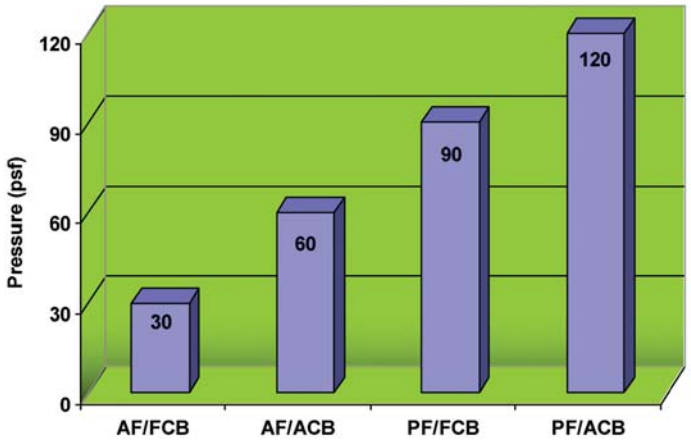

A) WIND UPLIFT RATING COMPARISON

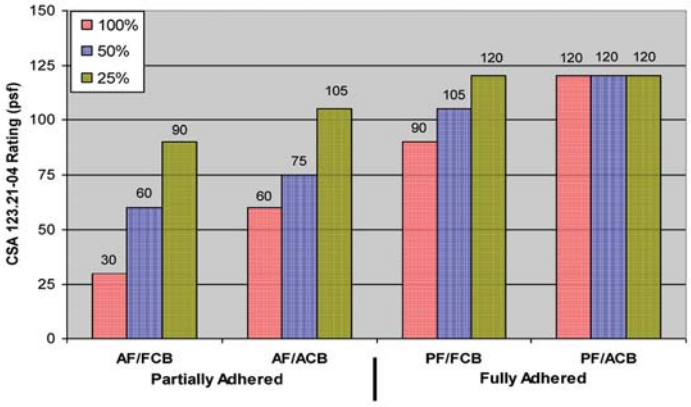

B) WIND UPLIFT RATING AT 25%, 50%, AND 100% OF CSA LOAD CYCLES

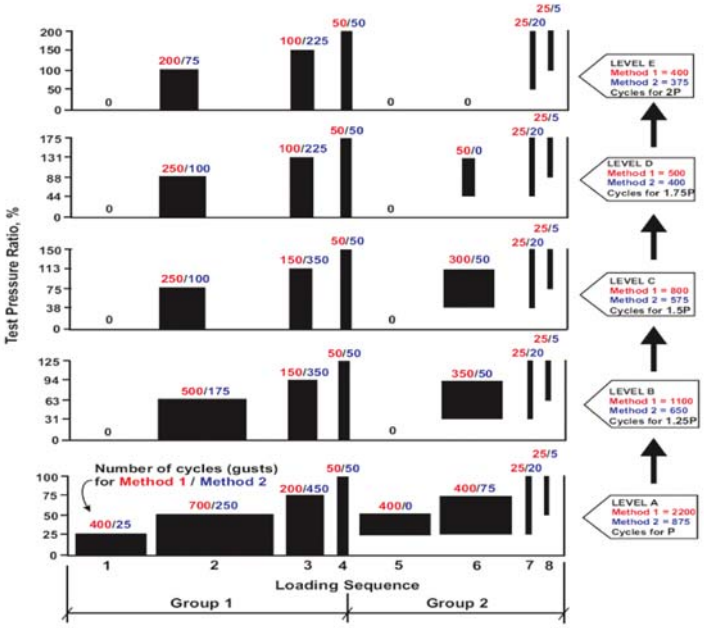

C) DYNAMIC LOAD CYCLES

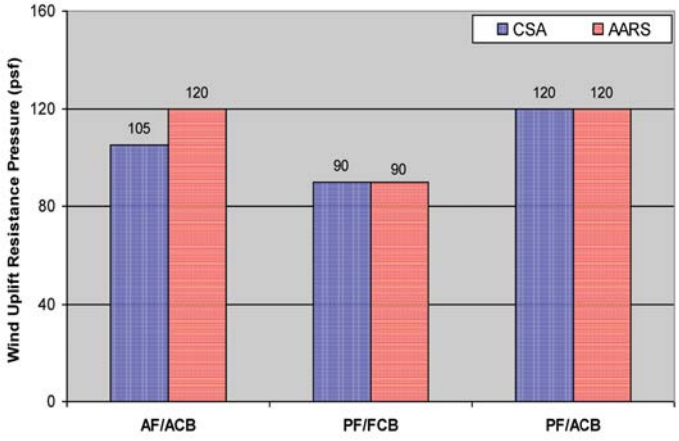

D) WIND UPLIFT RATING: CSA LOAD CYCLE VS. AARS LOAD CYCLES

Figure 8 – Determination of appropriate load cycles for AARS full-scale testing.

FULL-SCALE TESTING FOR WIND UPLIFT LOADING (MURTY, 2009)

Determination of Appropriate Load Cycle for Standardized Wind Uplift Test Protocol

To quantify the wind uplift ratings of MARS under dynamic loading conditions, they are presently tested in accordance with CSA 123.21-04. To develop a similar dynamic load cycle for the AARS, four mock-ups using two different types of insulation facers (paper and acrylic facers) and two different types of cover boards (asphalt core and fiber cover) were fabricated. The mock-ups can be labeled as AF/FB, AF/ACB, PF/FCB, and PF/ACB, in which AF, PF, ACB, and FCB stand for the acrylic facer insulation, paper facer insulation, asphalt core board, and fiberboard, respectively. Investigations started with the CSA load cycle.

Figure 8a shows the wind uplift resistance. Data show that the highest wind uplift resistance was achieved by the PF/ACB combination, whereas the poorest performance was by the AF/FCB combination. In addition, the test results also illustrate that the use of paper facer insulation resulted in superior wind uplift resistance in comparison to the use of acrylic facer insulation. This concludes that material combinations play an important role in the wind uplift resistance of the AARS.

To study the influence of a number of dynamic load cycles (gusts) on the performance of wind uplift resistance, eight additional mock-ups were fabricated and tested by using 25% and 50% of CSA load cycles. *Figure 8b* shows the variations in the wind uplift resistance ratings. Data illustrate that dynamic load cycles (gusts) can influence the wind uplift resistance; hence, it is necessary to determine the appropriate number of cycles for testing of AARS.

By following the procedure used for the MARS load-cycle development (Baskaran *et al.*, 1999), wind-tunnel data were gathered using rigid models. Pressure/time histories were collected for three different roof zones: field, edge, and corner. Tested rigid models varied in building heights and aspect ratios. gDirectional changes in the approaching wind and its impact on the induced pressures were also accounted for during the wind-tunnel testing. *Figure 8c* illustrates the newly developed load cycle for the rigid system. For comparative purposes, the load cycles suitable for the flexible systems are

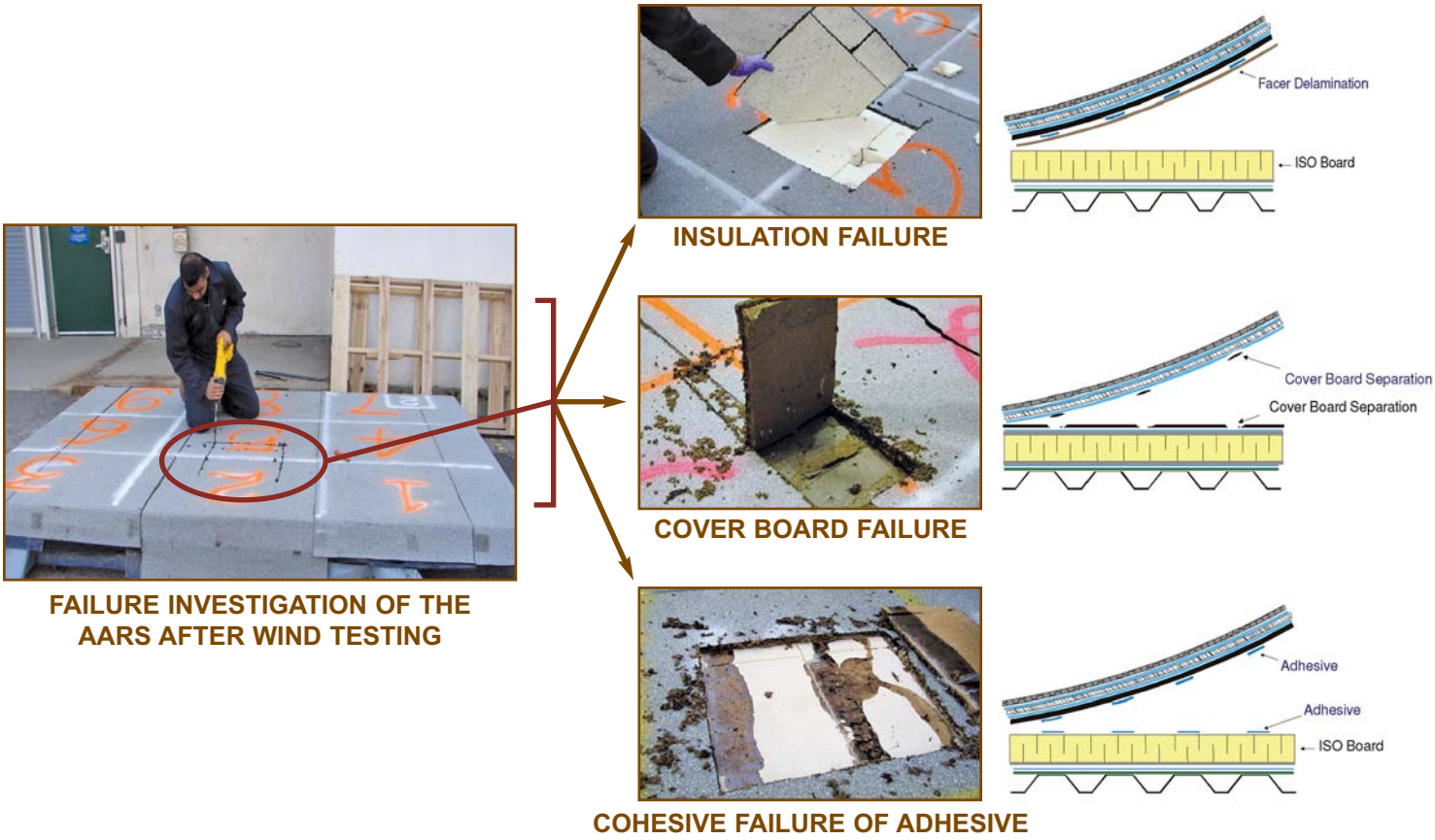

Figure 9 – Weakest link under wind uplift loading: a summary of failure mode analysis.

also included. They are labeled as Method 1 and Method 2 load cycles, respectively, for flexible and rigid systems. *Figure 8d* compares the wind uplift performance obtained by applying Method 1 and Method 2 load cycles.

Test results indicate that the mock-ups generally had similar wind uplift resistance, regardless of the load cycles applied. However, the Method 2 load cycle is more appropriate for the quantification of AARS wind uplift resistance because its testing time is faster than that of Method 1. Similar observations were also recorded when Method 1 was developed and compared with the standard practiced in Europe (ETAG-2006).

Weakest Link Under Wind Uplift Loading – Summary of Failure Mode Analysis

Failure modes were found to be similar among the full-scale test, uplift test, and peel test, which are insulation facer, delamination failure, fiberboard separation failure, and adhesive failure. *Figure 9* shows the typical weakest-link photos and diagrams for the common failure modes from the full-scale test.

Based on this study, it was determined that the weakest links are either the insulation board and/or the cover board. The insulation facer failure normally took place in any of the AARS configurations when asphaltic core board was used as the cover board. When fiberboard was used, however, it separated and became the weakest link, while the adhesive failure normally appeared if the mock-up was not totally cured.

Note that the weakest links presented herein are based on the research investigation results on the use of two types of cover boards (asphaltic core and fiberboards) and two types of isocyanurate insulation facers (paper and acrylic facers). Other possible failure modes may occur as a result of different components used in the configuration.

CONCLUDING REMARKS

Adhesive-applied roofing systems are currently used as alternatives in low-slope applications and employ no fasteners for component integration. Since AARS's response to wind uplift differs from conventional mechanically attached systems, NRC developed the following test protocols and submitted them as standardized processes.

1. *Standard Test Method for the Dynamic Wind Uplift Resistance of Membrane Roofing Systems*, CSA 123.21-04. This has been reissued.
2. *Standard Test Method for Determining the Uplift Resistance of Adhesive-Applied Roofing Systems*, ASTM Work Item WK26082, Task Group D08.20.37. This is in the balloting process for renewal.
3. *Standard Test Method for Determining the Peel Resistance of Adhesive-Applied Roofing Systems*, ASTM Work Item WK26083, Task Group D08.20.37. This is in the balloting process for renewal.

ACKNOWLEDGEMENT

The authors acknowledge the financial support provided by the Natural Sciences and Engineering Research Council (NSERC) project under Grant #CDR305819; roofing manufacturers Soprema, Inc.; Bakor, Inc.; TREMCO, Inc.; and IKO Industries, Ltd.; and the Roofing Contractors' Association of British Columbia (RCABC).

REFERENCES

A. Baskaran, Y. Chen, A. Vilaipornsawai, "A New Dynamic Wind-Load Cycle to Evaluate Flexible Membrane Roofs," *Journal of Testing and Evaluation*, Vol. 27, (4), July 1999, pp. 249-265.

A. Baskaran and T.L. Smith, *A Guide for the Wind Design of Mechanically Attached Flexible Membrane Roofs*, Institute for Research in Construction, National Research Council of Canada, Ottawa, Canada K1A OR6, 2005, ISBN 0-660-19518-6.

Canadian Standard Association, *Standard Test Method for the Dynamic Wind Uplift Resistance of Mechanically Attached Membrane Roofing Systems,* CSA 123.21-04, Toronto, 2004.

J. Current, "Development of a Pull-Out Test Method for Adhesive-Applied Roofing Systems," master's thesis, Department of Civil Engineering, University of Ottawa, 2009.

H. Hens, A. Janssens, and A. Silberstein, "A Study of Parameters Influencing the Hydric Behavior of Insulated, Sloped Roofs Without Air Barriers," *Thermal Envelopes Conference*, Vol. 1, pp. 729–739, 1995.

B. Murty, (2009), "Wind Uplift Performance Evaluation of Adhesive-Applied Roofing Systems," PhD thesis, Department of Civil Engineering, University of Ottawa, 2010.

J. Wu, "Development of a Peel-Test Procedure for Adhesive-Applied Roof Systems," master's thesis, Department of Civil Engineering, University of Ottawa, 2008.

Dr. A. "Bas" Baskaran, PEng

Dr. A. "Bas" Baskaran is a group leader and senior research officer at the National Research Council of Canada, Institute for Research in Construction (NRC/IRC). He has been immersed for 25 years in researching the wind effects on building envelopes through wind tunnel experiments and computer modeling. He also acts as adjunct professor at the University of Ottawa. Dr. Baskaran is a member of RCI, ASCE, SPRI RICOWI, ICBEST, and CIB technical committees. His work in the area of wind engineering and building envelopes has received national and international recognition. Baskaran has published more than 150 articles in peer reviewed journals and conference proceedings. A professional engineer, Baskaran received his master's degree in engineering and his doctorate from Concordia University, Montreal, Canada. Both research topics focused on the wind effects on buildings and earned best dissertation awards from the Canadian Society of Civil Engineers.

Hiroshi Tanaka

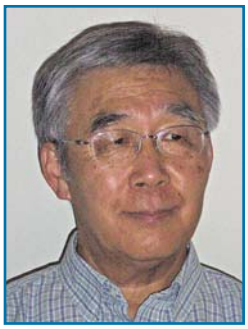

Hiroshi Tanaka received his education in Tokyo, Japan. After seven years at the Boundary Layer Wind Tunnel Laboratory, University of Western Ontario, working on research projects in wind engineering and structural dynamics, he joined the engineering faculty at the University of Ottawa in 1979, where he carried out teaching, research, and administrative duties until 2006. He is currently a professor emeritus there. He has published over 200 scientific papers in the field of wind engineering. As a consultant, he has been involved in wind-resistant design of many significant bridges worldwide, including the Great Belt Bridge in Denmark. He also worked as a guest researcher at the National Research Council Canada, Danish Maritime Institute, and Vienna Consulting Engineers.